25. Zahs, K. R. & Stryker, M. P. The projection of the visual field onto the lateral geniculate nucleus of the ferret. *J. Comp. Neurol.* **241**, 210–224 (1984).

Acknowledgements

We thank C. Waite for help with figures and data analysis; R. P. Dolan for help in designing the apparatus for experiment 1 and software; M. Ter-Minassian for helping with ferret training; R. Held and A. Roe for comments and suggestions throughout experiment 1; R. Marini for help with the surgical procedures and with animal care; R. Held, J. Rauschecker, C. Hohnke, A. Lyckman and J. Schummers for comments on the manuscript; and members of the Sur laboratory for advice and comments. We are particularly grateful to W. Singer for help and support during experiment 2. Supported by a fellowship from the Human Frontiers Science program (L.v.M.), a fellowship from the National Eye Institute (S.L.P.) and grants from the NIH (M.S.).

Correspondence and requests for materials should be addressed to M.S. (e-mail: msur@ai.mit.edu).

Experience-dependent plasticity of dendritic spines in the developing rat barrel cortex *in vivo*

Balazs Lendvai*, Edward A. Stern, Brian Chen & Karel Svoboda

Cold Spring Harbor Laboratory, 1 Bungtown Rd, Cold Spring Harbor, New York 11724, USA

Do changes in neuronal structure underlie cortical plasticity[1,2]? Here we used time-lapse two-photon microscopy[3,4] of pyramidal neurons in layer 2/3 of developing rat barrel cortex[5] to image the structural dynamics of dendritic spines and filopodia. We found that these protrusions were highly motile: spines and filopodia appeared, disappeared or changed shape over tens of minutes. To test whether sensory experience drives this motility we trimmed whiskers one to three days before imaging. Sensory deprivation markedly (~40%) reduced protrusive motility in deprived regions of the barrel cortex during a critical period around postnatal days (P)11–13, but had no effect in younger (P8–10) or older (P14–16) animals. Unexpectedly, whisker trimming did not change the density, length or shape of spines and filopodia. However, sensory deprivation during the critical period degraded the tuning of layer 2/3 receptive fields. Thus sensory experience drives structural plasticity in dendrites, which may underlie the reorganization of neural circuits.

More than 90% of excitatory axodendritic synapses in the mammalian cortex occur on small dendritic appendages called spines[6]. During development the emergence of spiny dendrites is preceded by a period when dendrites are studded with filopodia[7], relatively long (up to 10 μm) actin-rich protrusions which often make several synapses[8]. In the cerebral cortex the presence of dendritic filopodia coincides with an intense burst of synaptogenesis[9,10]. In cultures of developing hippocampus, dendritic filopodia are highly motile[11,12] and initiate contact with axons, leading to synapse formation[13]. Mature spines, on the other hand, are structurally relatively stable[13,14]. These observations support the idea that filopodia actively search for presynaptic partners and might in fact be precursors of mature spines[11–13]. Filopodia[12] and spines[15,16] sprout in response to strong synaptic stimuli that produce long-term potentiation, suggesting that such motility may be an important aspect of activity-dependent synaptic plasticity.

To explore the role of protrusive motility in the plasticity of neural circuits, experiments in the intact brain are necessary. For this purpose we imaged the dynamics of spines and filopodia in the developing primary vibrissa (barrel) cortex[5] of the rat. Modulating the sensory input to the barrel cortex by trimming whiskers changes the response properties of cortical neurons[2,17,18]. This allowed us to examine the effects of the rat's sensory experience on the structure and dynamics of spiny protrusions as a substrate of experience-dependent plasticity.

To label neurons for fluorescence imaging we injected a suspension of Sindbis virus containing the gene for enhanced green fluorescent protein (SIN–EGFP)[12,19] along the medial edge of the barrel cortex. Typically tens to hundreds of neurons, distributed over all cortical layers and over one to three barrels, were infected by the virus. One to two days after infection, EGFP had reached concentrations sufficiently high for imaging. Visualized with a custom-made two-photon laser scanning microscope (2PLSM), infected barrel cortex neurons showed bright EGFP fluorescence that was distributed homogeneously throughout their dendritic and axonal arborizations (Fig. 1a). High-resolution structure could be seen down to the level of dendritic spines and presynaptic terminals (Fig. 1b).

We examined the structures of layer 2/3 pyramidal neurons, as they are within easy reach of our imaging technique (imaging depth < 600 μm)[20] and also because in the adult they show the most pronounced form of experience-dependent plasticity[17,18]. In addition we focused our observations on postnatal day 8 to 18, a period that spans the development of much of the intracortical circuitry[9].

To characterize the dynamics of spiny protrusions *in vivo* we performed time-lapse imaging in anaesthetized rats (Fig. 2A, B). Small image stacks containing a particular dendritic branch were typically collected at 10-min intervals for at least 90 min (Fig. 2Aa, Ba). Motility was quantified by measuring the length of individual protrusions as a function of time (Fig. 2Ab, Bb). Sampling intervals of 10 min were sufficient to capture most protrusive movements (Fig. 2Ab); occasional experiments with more frequent data collection (1 min) showed little additional structural change over shorter timescales (Fig. 2Ab). To describe the structural dynamics for an individual protrusion we use the average change of length per sampling interval (micrometres per 10 min).

Time-lapse imaging revealed that spines and filopodia are highly motile *in vivo* (Fig. 2A–C). They changed length and shape over tens of minutes. In addition to length and shape changes, a significant proportion (2–20%) of protrusions appeared or disappeared during the observation period (Fig. 2A, B). The largest motility was observed in the youngest animals probed (P8–12; Fig. 2C). At these ages dendritic structure was characterized by numerous irregular spiny protrusions, with a relatively large fraction of long filopodia (length >4.5 μm; ~6–7%; Fig. 2D). With increasing age protrusive motility decreased (Fig. 2C). In older animals (P16–19) dendritic structure was characterized by spines typical of mature dendrites (Fig. 2Ba), with relatively few long filopodia (1–2%; Fig. 2D).

Previous *in vitro* studies have established that the protrusive motility of spines and filopodia indicates a rapid rearrangement of synaptic connections and neural circuits[12,13,15,16]. To investigate the role of sensory experience in this plasticity we examined the effects of sensory deprivation on the structure and dynamics of spiny protrusions. Deprivation was induced 1–3 days before imaging by trimming all large whiskers (columns 1–4, α–δ) on one side of the rat's muzzle, contralateral to the injection site. We compared dendritic structure and dynamics under three conditions (Fig. 3a). To assess the effects of deprivation, imaging was performed in control (left, 'in, control') or deprived (middle, 'in, deprived') barrel cortex. To test whether the effects of deprivation are specific to the deprived input, imaging was performed in the trunk, back and head regions of somatosensory cortex[21], <1 mm medial to deprived barrel cortex (right, 'out, deprived'). The locations of

* Present address: Institute of Experimental Medicine, Hungarian Academy of Sciences, Szigony u. 43, 1083 Budapest, Hungary.

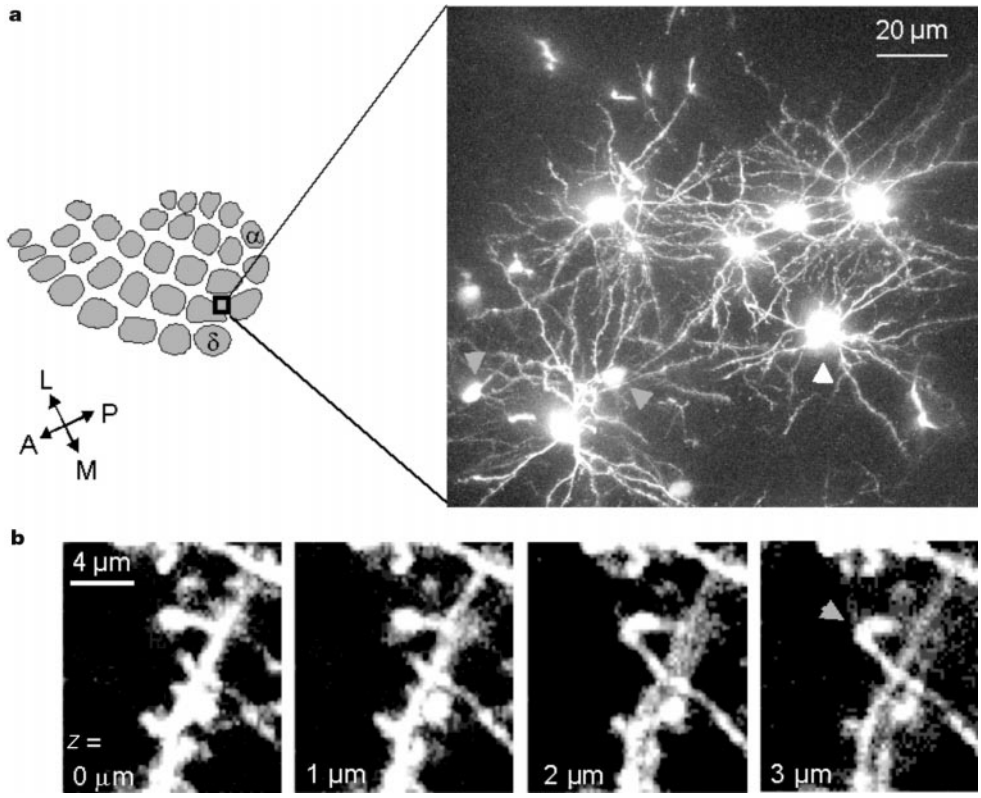

Figure 1 High-resolution imaging of barrel cortex neurons infected with SIN–EGFP *in vivo*. **a**, Left, schematic representation of the barrel field. Injections were made along the medial edge. Right, 2PLSM image of cluster of infected layer 2 neurons (white arrow heads) with basal dendrites (P11, 2 days after infection; projection of 30 sections, 220–280 µm below the surface of the brain). Note the cross-sections of thick apical dendrites belonging to deep pyramidal cells (grey arrowheads). **b**, High resolution 2PLSM images showing apparent contact between a dendritic segment and an axon. Four optical sections separated by 1 µm are shown.

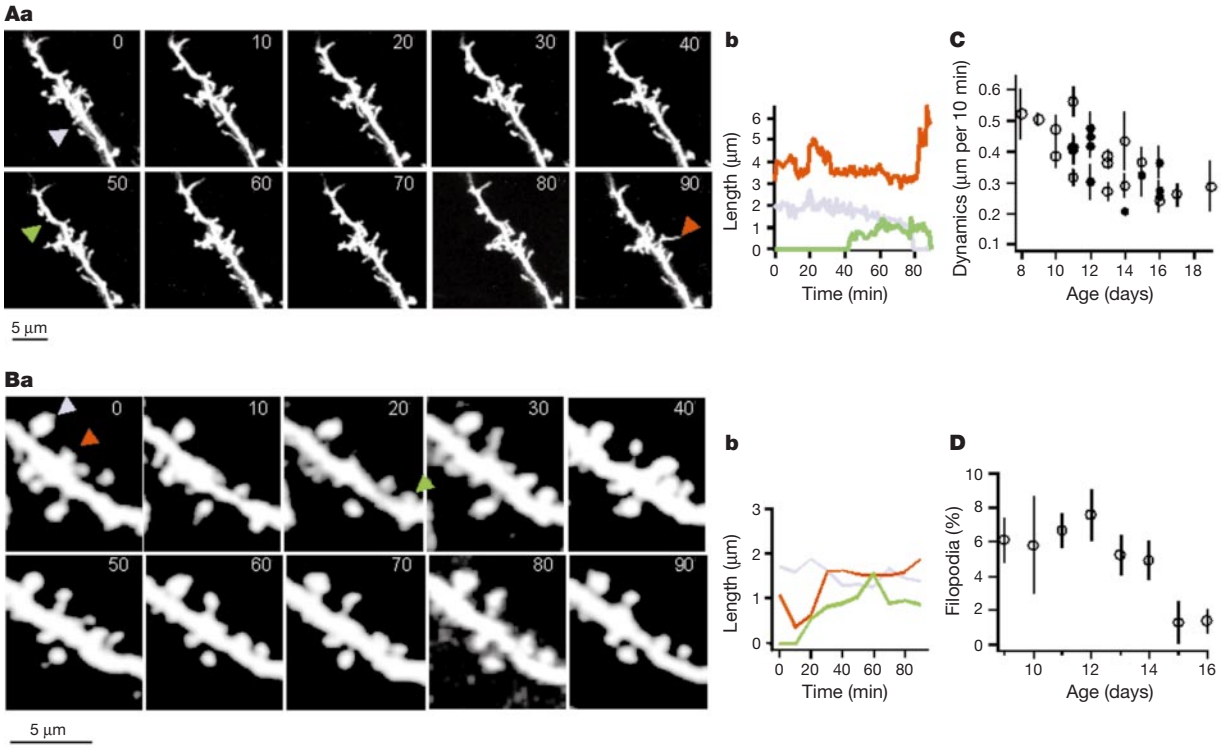

Figure 2 Motility of dendritic protrusions and their developmental regulation. **Aa, Ba**, Time-lapse image sequences showing growth, retraction and other shape changes of dendritic protrusions (time stamps are in min). Coloured arrows point to protrusions that are analysed further in the right panels. Conditions: **A**, imaging rate 1 min^{-1}, P11, control; **B**, imaging rate 1/10 min^{-1}, P17, control. **Ab, Bb**, Time courses of length of selected protrusions. **C**, Development of motility of protrusions. Measurements in barrel cortex of control animals (closed circles) and outside barrel cortex in deprived animals (open circles) are shown. **D**, Fraction of protrusions classified as filopodia (length >4.5 µm).

imaged neurons with respect to barrel cortex were determined histologically (Fig. 3b). In addition, we performed experiments on three age groups: during (P11–13), before (P8–10) and after (P14–16) a brief period of rapid synaptogenesis (P11–14) when cortical synapse number increases by 400%[9]. Concurrent with this rapid synaptogenesis rats begin to use their whiskers in exploratory behaviours[22].

Time-lapse imaging revealed that protrusive motility is modulated by previous experience, but only during a brief cortical critical period, P11–13. During this period, deprivation caused a large decrease in motility (Fig. 3c; −37%, corrected for baseline movement; control, 0.40 ± 0.01 μm per 10 min; deprived, 0.29 ± 0.01 μm per 10 min). Analysing different classes of protrusions separately revealed that deprivation significantly reduced the motility of long filopodia (Fig. 3d; −49%; control, 0.81 ± 0.04 μm per 10 min; deprived, 0.46 ± 0.06 μm per 10 min) as well as spines (Fig. 3e; −36%; control, 0.34 ± 0.01 μm per 10 min; deprived, 0.25 ± 0.01 μm per 10 min). Protrusions located in regions adjacent to deprived barrel cortex did not show reduced motility (Fig. 3c–e), indicating that the effects of sensory deprivation are specific to the deprived region of the cortex. Experiments in older (P14–16; Fig. 3f) and younger (P8–10; Fig. 3g) animals also failed to show experience-dependent effects on protrusive dynamics; similar results were found when spines and filopodia were analysed separately (data not shown).

As deprivation reduces protrusive motility at P11–13, it might be expected that deprivation would perturb the shapes and densities of dendritic protrusions. But comparing dendrites in deprived and control barrel cortex at P11–13 revealed that deprivation produced no obvious differences in spiny structure on average (Fig. 4a, b). The densities of protrusions (Fig. 4a), distributions of protrusion lengths (Fig. 4b) and distributions among different morphological classes of protrusions (Fig. 4c, d) were unchanged by sensory deprivation. Similar results were obtained for older (P14–16) and younger (P8–10) animals (data not shown). Thus, there is a critical period (P11–13) when experience can influence the stability of dendritic protrusions in layer 2/3, without perturbing their density

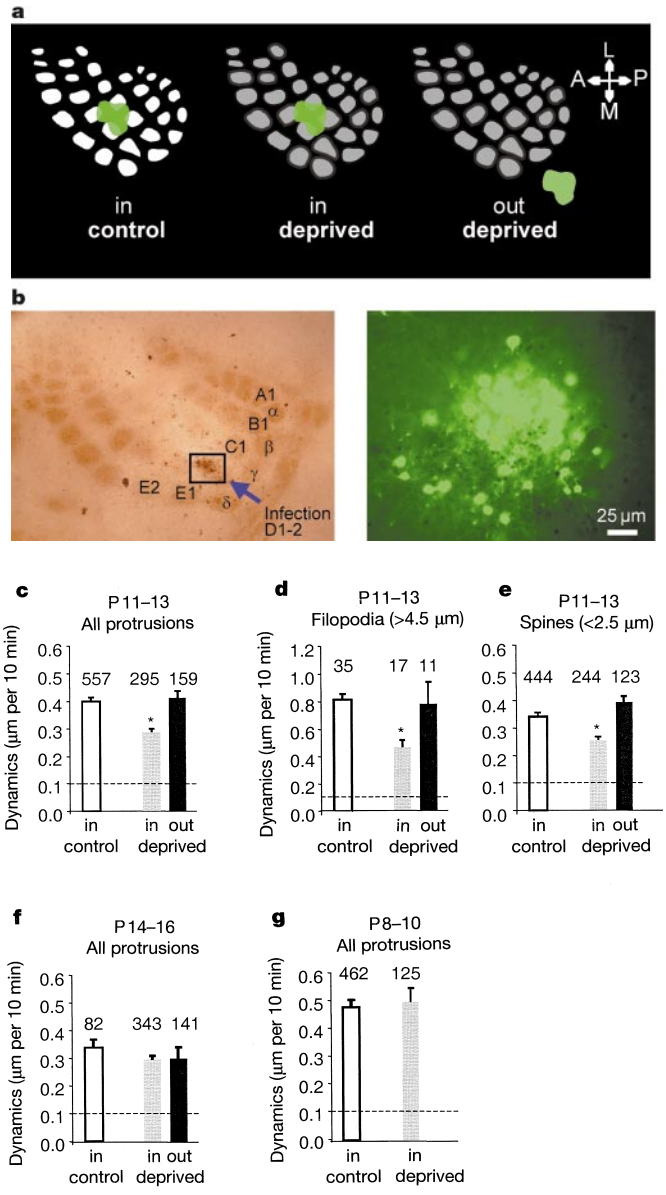

Figure 3 Effects of sensory deprivation on the motility of spiny protrusions. **a**, Schematic representation of experimental treatments. Left, control animals (white barrels) with viral infection (green blotch) and imaging in the barrel field. Middle, deprived animals (grey barrels) with viral infection and imaging in the barrel field. Right, deprived animals with viral infection and imaging outside the medial edge of the barrel field. **b**, Histological analysis of the injection site. Left, brightfield image of layer 4 tangential flattened section stained for cytochrome oxydase (thickness ~100 μm) showing the arrangement of the barrel field. Infected neurons appear as dark spots (arrow). Right, fluorescence image of an enlargement of the same section showing infected neurons. **c–g**, Dynamics in control (open bars), deprived barrel cortex (grey bars) and outside deprived barrel cortex (black bars). Dashed lines indicate the noise floor. Protrusion numbers are indicated above bars. **c–e**, P11–13. **c**, Whisker trimming depresses the dynamics of dendritic protrusions in the P11–13 group (asterisk, $P < 10^{-7}$). **d**, Only filopodia (asterisk, $P < 10^{-2}$, subset of **c**). **e**, Only spines (asterisk, $P < 10^{-5}$, subset of **c**). **f**, Whisker trimming does not affect the dynamics of dendritic protrusions in the P14–16 group ($P > 10^{-1}$). **g**, Whisker trimming does not affect the dynamics of the of dendritic protrusions in the P8–10 group ($P > 10^{-1}$).

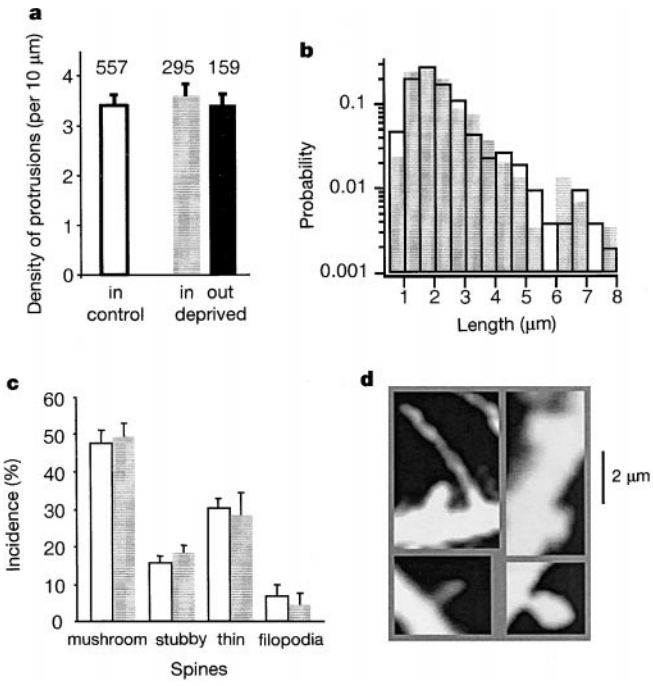

Figure 4 Whisker trimming does not change the structure of spines and filopodia (P11–13). **a**, Density of protrusions. **b**, Distribution function of lengths of dendritic protrusions (grey bars, deprived; open bars, control; Kolmogorov–Smirnov two-sample test, $P > 0.1$). **c**, Protrusions classified by type[6] in control (open bars) and deprived (grey bars) barrel cortex. The error bars were computed over number of dendritic branches ($n = 150$). **d**, Examples of protrusions as classified for the histogram in **c**. Clockwise from top left: Filopodia, stubby spines, mushroom spines, thin spines.

or shape. As protrusive motility correlates with synaptogenesis[13], our findings indicate that during this critical period experience modulates synaptic lifetimes, without changing synaptic densities. Experience-dependent morphogenesis might therefore be a structural correlate of the synaptic pruning and growth required for the tuning of sensory maps.

Does sensory deprivation during the critical period perturb the development of barrel cortex maps? We examined the effects of whisker trimming on the development of layer 2/3 receptive fields. We used sharp microelectrodes to record the membrane potential dynamics of regular spiking neurons in P14–16 rats (neurons in and around barrel C3 were targeted). The amplitudes of postsynaptic potentials (PSPs) were measured in response to deflections of single whiskers. In control brains sensory maps resembled those measured in adult animals[23,24] (Fig. 5A). The PSP was largest in response to deflections of one dominant whisker (the principal whisker, PW, 5.8 ± 1.4 mV, $n = 4$). Surround whiskers (SW) produced a comparatively small response (Fig. 5A, C). These well-tuned sensory maps stand in contrast to those recorded in animals that had their whiskers trimmed from P10 to P15 (Fig. 5B). In these animals the principal whisker response (defined as the largest response) was smaller than in control animals (3.2 ± 1.4 mV, $n = 5$), but the surround was stronger and broader (Fig. 5B, C; $P < 0.001$, randomization test for independent samples). Thus sensory deprivation spanning the critical period has a profound effect on the tuning of sensory maps of layer 2/3 pyramidal neurons.

In brain slices, spines and filopodia sprout in response to strong synaptic stimulation[12,15,16]. It is thus possible that experience-dependent changes in spontaneous synaptic activity drive changes in protrusive motility at the time of imaging. To address this issue we measured membrane potential fluctuations in the developing barrel cortex (Fig. 5D–Ga). Network synaptic activity was quantified by computing the distribution of membrane potentials (Fig. 5D–Gb), where the widths of these distributions measure the strength of synaptic activity. Consistent with the increase in synaptic densities expected during development from P11–13 to P14–16, membrane potential distributions increased in width (P11–13, 5.2 ± 0.5 mV, $n = 5$; P14–16, 12.7 ± 0.5 mV, $n = 5$; $P < 0.001$). However, sensory deprivation did not change the widths of distributions either in P11–13 (control, 5.2 ± 0.5 mV; deprived, 5.5 ± 0.9 mV, $n = 4$; $P > 0.1$) or P14–16 (control, 12.7 ± 0.5; deprived, 13.3 ± 0.5, $n = 5$; $P > 0.1$) animals. Thus deprivation did not have obvious long-lasting effects on network synaptic activity and experience-dependent changes in motility are coupled more directly to the history of sensory activity.

In conclusion, we have used time-lapse imaging to show that dendritic protrusions are dynamic over timescales of 10 min and over lengths of micrometres (Fig. 2). These results are in agreement with those of experiments on hippocampal pyramidal cells in cultured brain slices[11,12]. Experiments on cultured hippocampal neurons[25] have shown fast (seconds) actin-powered spine dynamics over much smaller distances, while experiments on cultured brain slices from ferret visual cortex report relatively stable spines[14]. Differences in preparation or developmental age could explain the

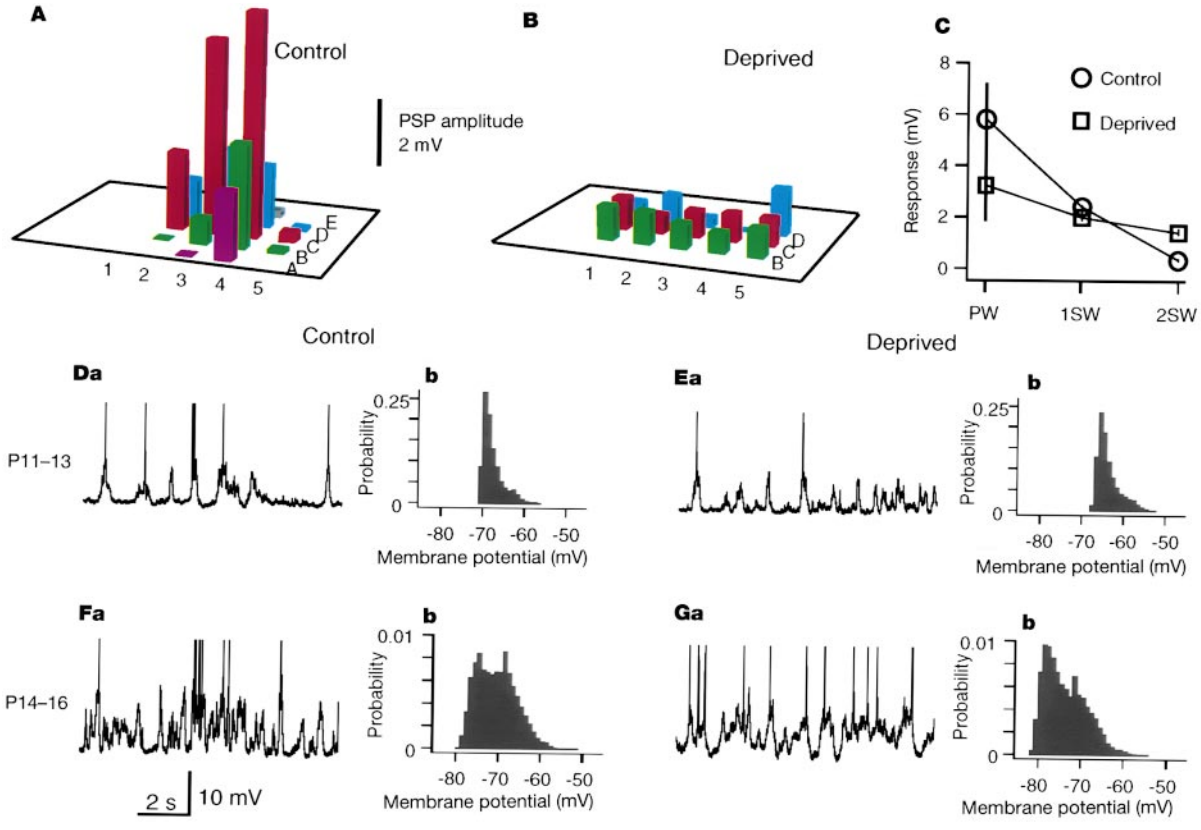

Figure 5 Electrophysiology of layer 2/3 neurons. **A–C**, The effects of deprivation on the average postsynaptic potentials (PSPs) evoked by different whiskers (columns 1–5, rows A–E) (P14–16). **A**, Typical sensory map from a neuron in a control animal showing a dominant principal whisker and sharp tuning. **B**, Map from a neuron in a deprived animal showing typically poor tuning. **C**, Tuning of sensory maps in control (circles, $n = 4$) and deprived (squares, $n = 5$) (the principal whisker (PW) response was defined as the largest response; nearest neighbours (surrounding whiskers) 1SW; next nearest neighbours 2SW; difference between trends, $P < 0.001$). **D–G**, Effects of deprivation on spontaneous synaptic activity. **a**, Representative examples of spontaneous activity. Note that action potentials are cut off. **b**, Representative examples of distributions of membrane potentials. Spontaneous activity in deprived (**D**) and control (**E**) animals showed no differences in P11–13 animals ($P > 0.1$). Spontaneous activity in deprived (**F**) and control (**G**) animals showed no differences in P14–16 animals ($P > 0.1$).

discrepancies between these *in vitro* studies and our *in vivo* observations. Consistent with previous studies[10,11,13], we find that dendritic filopodia are especially common during periods of rapid synaptogenesis (Fig. 2D).

Sensory deprivation can depress the motility of spines and filopodia (Fig. 3c–e) but does not appear to change the average structure or density of these protrusions (Fig. 4). These results indicate that sensory deprivation does not modulate synapse number itself, but perturbs the experience-dependent rearrangements of synaptic connections required to form precise sensory maps. However, further experiments will be necessary to establish the connection between protrusive dynamics and synaptogenesis directly. Our observation of experience-independent dendritic structure is consistent with anatomical studies showing that sensory deprivation during development does not change synaptic densities in visual[26] or barrel[27] cortex. Experience-dependent modulation of dendritic motility is limited to a sharp critical period (P11–13) and sensory deprivation during this period is associated with defective development of layer 2/3 sensory maps (Fig. 5A–C) (see also refs 28, 29). It should be noted that the critical period we describe is distinct from the critical period during which barrel structure can be modulated by damage to the sensory periphery[30]. Thus, sensory experience drives dendritic motility that is involved in the reorganization of cortical circuits, probably by competition between barrels[18]. As protrusive motility correlates with rates of synaptogenesis[13], our study implies that experience-dependent plasticity may, at least in part, be encoded by formation of new synaptic connections rather than modification of existing synapses[2]. □

Methods

Infection of neocortical neurons *in vivo*

All surgery was performed in accordance with the animal care and use guidelines of CSHL. One to three days before imaging, rats ($n = 45$) were anaesthetized with a ketamine/xylazine cocktail (ketamine: 0.56 mg g^{-1} body weight; xylazine: 0.03 mg g^{-1} body weight). Glass pipettes (tip diameter ~12 μm) were used to inject virus (SIN–EGFP) into the brain parenchyma. Sensory deprivation was initiated by trimming (to < 1 mm) all large whiskers (columns 1–4, α–δ). The effects of trimming 1, 2 or 3 days before imaging were indistinguishable (data not shown). The age groups for the deprivation experiments at the time of imaging were as follows (number control/number deprived): P8–10, 4/5; P11–13, 5/9; P14–16, 5/9. Levene's test (analysis of variance on absolute deviations) revealed that individual animals at the same age and in the same treatment group were not significantly different ($P \approx 0.15$). We therefore quote the number of protrusions as the sampled size, n.

We tested whether the viral protein itself could produce abnormal morphology. Dendritic morphologies of neurons infected with SIN-EGFP were compared with neurons labelled with DiO. No differences were found up to four days after infection (data not shown).

In vivo two-photon laser scanning microscopy

At least one day and not more than three days after infection, rats were anaesthetized with ketamine/xylazine and prepared for imaging as described[20]. *In vivo* 2PLSM imaging was achieved using a custom-designed microscope. The specimen was rigidly attached to the optical bench for maximal stability. As a light source we used a Ti:sapphire laser (Tsunami, Spectra Physics) pumped by a 10-W solid state laser (Millenia X, Spectra Physics). The objective (40 ×, 0.8 numerical aperture) and scan lens were from Zeiss, the trinoc from Olympus and the photomultiplier tube from Hamamatsu. Image acquisition was achieved with custom software (Bell Laboratories, Lucent Technologies).

Data acquisition and analysis

In each animal 3–4 regions (field of view ~ 110 × 110 μm^2) were selected for imaging, each containing 1–3 analysed dendritic branches (length 34 ± 11 μm, mean ± s.d., $n = 290$). Small image stacks (10–20 images, z-spacing ~1 μm) were collected in each region every 10 min. More than half of the imaged dendrites were from identified layer 2/3 neurons. The somata belonging to the other half of the dendrites could not be positively identified; a small fraction could have been from layer 5 neurons.

Images were analysed off-line, essentially unprocessed, using custom software. The analyser was blind to the location of the injection (within or outside the barrel field). The numbers and lengths (base to tip; lower limit ~0.2 μm) of protrusions were measured, keeping track of the fates of individual structures. Conservative criteria were used to define filopodia as protrusions that reach a length of at least 4.5 μm during the observation period. Structures were classified as spines if their lengths never exceeded 2.5 μm. Published criteria were used to group spines into morphological classes[6] (Fig. 4c, d).

Structural measurements were done in small projections (~5 sections). Protrusions that pointed up or down from the dendrite were not detected because of the limited z-resolution (~2 μm) of our microscope. As measurements were done in two-dimensional projections, the quoted lengths of protrusions constitute an underestimate of the true lengths.

To characterize movement associated with breathing or heartbeat we imaged individual dendritic segments rapidly (every 20 s). This sampling interval is sufficiently long for heartbeat (~5 Hz) and breathing (~2 Hz) movement to produce displacement. Little movement was observable over these timescales (0.1 ± 0.02 μm per 20 s). This number is equal to the measurement error, characterized as the s.d. of the length measurement for the same structure measured repeatedly in the same image (0.1 μm). Therefore the larger dynamics we observed over longer timescales were due to dendritic motility. Measures of structural dynamics for protrusion k were computed as $|d|_k = \frac{1}{N}\Sigma_{t=0,T-\delta}|x_{k,t+\delta} - x_{k,t}|$. T is the observation period, δ is the time interval between time points, and N is the number of intervals ($N = T/\delta$).

One concern is that our measurements may have been perturbed by the effects of anaesthesia. Addressing this issue will ultimately require imaging in awake animals. However, in control experiments using urethane ($n = 2$), an anaesthetic with a different pharmacological profile than ketamine, we find similar protrusive motility (ketamine 0.41 ± 0.01 μm per 10min; urethane 0.45 ± 0.04 μm per 10 min, P11–13). Therefore it is unlikely that specific pharmacological effects due to the anaesthetic have perturbed our results. Tests for differences between populations were performed using the t-test unless indicated otherwise. Significance levels were set at $P = 0.05$. Measurements are given as mean ± s.e.m., unless indicated otherwise.

Intracellular recording *in vivo*

Rats (P13, $n = 9$; P15, $n = 15$) were anaesthetized by intraperitoneal injection of urethane (1.5 mg g^{-1}). The experimenter was blind to the deprivation. A sharp microelectrode (1 M potassium acetate) was inserted into the supragranular layer of the barrel field. All neurons (1–2 per animal) were regular spiking with somata between 200 and 500 μm below the pia and thus in layers 2/3. Sensory maps were constructed in P15 animals by stimulating whiskers with a piezoelectric actuator with 200 ms deflections at 1 Hz, for 10–30 trials. The response was defined as the PSP amplitude.

Received 20 December 1999; accepted 2 February 2000.

1. Bailey, C. H. & Kandel, E. R. Structural changes accompanying memory formation. *Annu. Rev. Physiol.* **55,** 397–426 (1993).
2. Buonomano, D. V. & Merzenich, M. M. Cortical plasticity: from synapses to maps. *Annu. Rev. Neurosci.* **21,** 149–186 (1998).
3. Denk, W., Strickler, J. H. & Webb, W. W. Two-photon laser scanning microscopy. *Science* **248,** 73–76 (1990).
4. Denk, W. & Svoboda, K. Photon upmanship: why multiphoton imaging is more than a gimmick. *Neuron* **18,** 351–357 (1997).
5. Woolsey, T. A. & van der Loos, H. The structural organization of layer IV in the somatosensory region (S1) of mouse cerebral cortex. *Brain Res.* **17,** 205–242 (1970).
6. Harris, K. M. & Kater, S. B. Dendritic spines: cellular specializations imparting both stability and flexibility to synaptic function. *Annu. Rev. Neurosci.* **17,** 341–371 (1994).
7. Purpura, D. in *Advances in Neurology* (ed. Kreutzberg, G. W.) 91–116 (Raven, New York, 1975).
8. Fiala, J. C., Feinberg, M., Popov, V. & Harris, K. M. Synaptogenesis via dendritic filopodia in developing hippocampal area CA1. *J. Neurosci.* **18,** 8900–8911 (1998).
9. Micheva, K. D. & Beaulieu, C. Quantitative aspects of synaptogenesis in the rat barrel field cortex with special reference to GABA circuitry. *J. Comp. Neurol.* **373,** 340–354 (1996).
10. Miller, M. & Peters, A. Maturation of rat visual cortex. II. A combined Golgi-electron microscope study of pyramidal neurons. *J. Comp. Neurol.* **203,** 555–573 (1981).
11. Dailey, M. E. & Smith, S. J. The dynamics of dendritic structure in developing hippocampal slices. *J. Neurosci.* **16,** 2983–2994 (1996).
12. Maletic-Savatic, M., Malinow, R. & Svoboda, K. Rapid dendritic morphogenesis in CA1 hippocampal dendrites induced by synaptic activity. *Science* **283,** 1923–1927 (1999).
13. Ziv, N. E. & Smith, S. J. Evidence for a role of dendritic filopodia in synaptogenesis and spine formation. *Neuron* **17,** 91–102 (1996).
14. Horch, H. W., Kruttgen, A., Portbury, S. D. & Katz, L. C. Destabilization of cortical dendrites and spines by BDNF. *Neuron* **23,** 353–364 (1999).
15. Engert, F. & Bonhoeffer, T. Dendritic spine changes associated with hippocampal long-term synaptic plasticity. *Nature* **399,** 66–70 (1999).
16. Toni, N., Buchs, P. A., Nikonenko, I., Bron, C. R. & Muller, D. LTP promotes formation of multiple spine synapses between a single axon terminal and a dendrite. *Nature* **402,** 421–425 (1999).
17. Diamond, M. E., Huang, W. & Ebner, F. F. Laminar comparison of somatosensory cortical plasticity. *Science* **265,** 1885–1888 (1994).
18. Fox, K., Glazewski, S., Chen, C. M., Silva, A. & Li, X. Mechanisms underlying experience-dependent potentiation and depression of vibrissae responses in barrel cortex. *J. Physiol. (Paris)* **90,** 263–269 (1996).
19. Malinow, R. in *Imaging Living Cells* (eds Yuste, R., Lanni, F. & Konnerth, A.) 58.1–58.8 (Cold Spring Harbor Press, Cold Spring Harbor, 1999).
20. Svoboda, K., Denk, W., Kleinfeld, D. & Tank, D. W. *In vivo* dendritic calcium dynamics in neocortical pyramidal neurons. *Nature* **385,** 161–165 (1997).
21. Chapin, J. K. & Lin, C. S. in *The Cerebral Cortex of the Rat* (eds Kolb, B. & Tees, R. C.) 341–380 (MIT Press, Cambridge, Massachusetts, 1990).
22. Welker, W. I. Analysis of sniffing of the albino rat. *Behavior* **22,** 223–244 (1964).
23. Moore, C. I. & Nelson, S. B. Spatio-temporal subthreshold receptive fields in the vibrissa representation of rat primary somatosensory cortex. *J. Neurophysiol.* **80,** 2882–2892 (1998).
24. Zhu, J. J. & Connors, B. W. Intrinsic firing patterns and whisker-evoked synaptic responses of neurons in the rat barrel cortex. *J. Neurophysiol.* **81,** 1171–1183 (1999).
25. Fischer, M., Kaech, S., Knutti, D. & Matus, A. Rapid actin-based plasticity in dendritic spines. *Neuron* **20,** 847–854 (1998).

26. Winfield, D. A. The postnatal development of synapses in the visual cortex of the cat and the effects of eyelid closure. *Brain Res.* **206,** 166–171 (1981).
27. Vees, A. M., Micheva, K. D., Beaulieu, C. & Descarries, L. Increased number and size of dendritic spines in ipsilateral barrel field cortex following unilateral whisker trimming in postnatal rat. *J. Comp. Neurol.* **400,** 110–124 (1998).
28. Movshon, J. A. & Dursteler, M. R. Effects of brief periods of unilateral eye closure on the kitten's visual system. *J. Neurophysiol.* **40,** 1255–1265 (1977).
29. Simons, D. J. & Land, P. W. Early experience of tactile stimulation influences organization of somatic sensory cortex. *Nature* **326,** 694–697 (1987).
30. Schlaggar, B. L., Fox, K. & O'Leary, D. D. M. Postsynaptic control of plasticity in developing somatosensory cortex. *Nature* **364,** 623–626 (1993).

Acknowledgements

We thank B. Burbach and E. Nimchinsky for help with experiments, K. Greenwood for help with analysis, Z. Mainen, M. Maravall, E. Ruthazer and B. Sabatini for comments on the manuscript, and the Malinow laboratory for help with viruses. This work was supported by IBRO (BL), HFSP, the Mathers and Pew Foundations (K.S.) and an NIH training grant to SHNY Stony Brook (B.C.).

Correspondence and requests for materials should be addressed to K.S. (e-mail: svoboda@cshl.org).

Ion permeation mechanism of the potassium channel

Johan Åqvist* & Victor Luzhkov*†

* *Department of Cell and Molecular Biology, Uppsala University, Biomedical Center, Box 596, SE-751 24 Uppsala, Sweden*

Ion-selective channels enable the specific permeation of ions through cell membranes and provide the basis of several important biological functions; for example, electric signalling in the nervous system[1]. Although a large amount of electrophysiological data is available[1,2], the molecular mechanisms by which these channels can mediate ion transport remain a significant unsolved problem. With the recently determined crystal structure of the representative K^+ channel (KcsA) from *Streptomyces lividans*[3], it becomes possible to examine ion conduction pathways on a microscopic level. K^+ channels utilize multi-ion conduction mechanisms[1,2,4–6], and the three-dimensional structure also shows several ions present in the channel. Here we report results from molecular dynamics free energy perturbation calculations that both establish the nature of the multiple ion conduction mechanism and yield the correct ion selectivity of the channel. By evaluating the energetics of all relevant occupancy states of the selectivity filter, we find that the favoured conduction pathway involves transitions only between two main states with a free difference of about 5 kcal mol^{-1}. Other putative permeation pathways can be excluded because they would involve states that are too high in energy.

The KcsA channel is a membrane-spanning tetrameric assembly with a narrow selectivity filter for permeating ions near its extracellular side, as well as a relatively large water-filled cavity near the centre of the membrane[3] (Fig. 1). These two structural features provide a stabilizing environment for ions passing through the channel that allows them to surpass the high energy barrier otherwise imposed by the nonpolar membrane interior. The filter region, which corresponds to the highly conserved signature sequence (TVGYG), comprises four more-or-less distinct binding sites that are occupied by ions or water molecules. These sites are separated by 3.4 Å, 3.9 Å and 3.3 Å in the crystal structure (Protein Data Bank (PDB) entry 1bl8)[3] which sterically allows their simultaneous occupation by four particles (K^+ ions or water molecules, both with a typical radius of 1.4 Å). This four-site structure gives rise to 16 theoretically possible loading states of the filter (Fig. 2). The main problem in determining the ion conduction mechanism is thus to find the energetically most favourable pathway that connects a subset of these states in a cyclic fashion, resulting in a net translocation of ions across the membrane. It may be seen from the combinatorial scheme that there are several possible permeation cycles of varying complexity, involving different number of loading states. We consider here the inward flux direction as observed in typical patch-clamp experiments under hyperpolarized conditions[7]. Figure 2 depicts only the pathways that result from 'single-file' movement through the selectivity filter; that is, ions/waters occupying the four filter positions will then all be shifted inwards one step as an ion or water molecule moves into the first position, and the species occupying the fourth position is released into the cavity region.

Experimental current–voltage relationships for typical K^+ channels (including KcsA), as well as gramicidin, yield conductance values in the tens of picosiemens range[2,7,8]. When these results are interpreted in terms of kinetic barrier models for ion permeation, activation free energies of around 5–7 kcal mol^{-1} are predicted[1,2,8–12]. Although the qualities of different models for ion permeation are still under debate[12,13], this type of estimate does establish an upper limit for the energy barriers involved in the process. To find the operational translocation mechanism for K^+ ions, we calculated the relative free energies of different configurations in Fig. 2 with the molecular dynamics (MD) free energy perturbation (FEP) technique[14–16]. This involves the evaluation of free energies of binding ions from an external solution, as well as of permuting ion and water positions inside the filter. In all simulations the channel tetramer

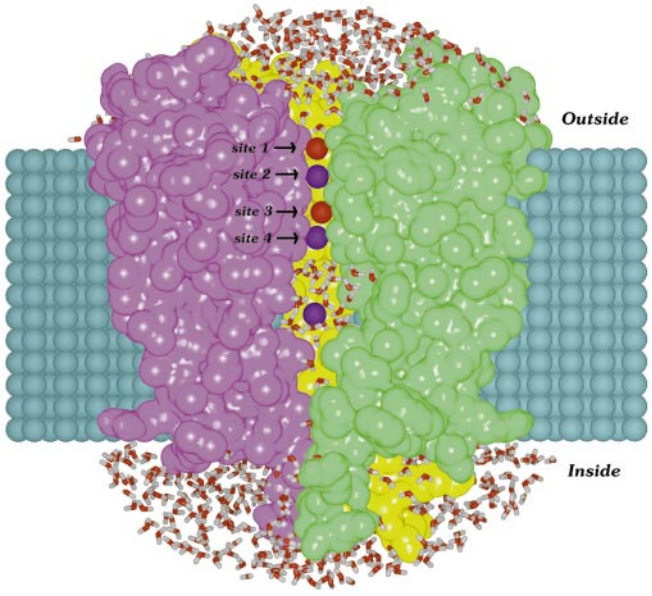

Figure 1 View of the solvated KcsA channel in which one of the four subunits has been omitted from the picture to make the pore visible. The filter region near the extracellular side is ~12 Å long with backbone carbonyl groups facing the pore, thereby providing stabilization of ions through interaction with their dipoles. The central cavity below the filter can accommodate a number of water molecules (around 30), and the diffuse electron density observed experimentally in this region shows the presence of a solvated ion[3]. The depicted structure has two water molecules (red spheres) and two ions (blue) in the selectivity filter and one in the central water-filled cavity. The channel is embedded in a cylindrical model membrane in all calculations.

† Permanent address: Institute of Chemical Physics Problems, Russian Academy of Sciences, Chernogolovka, Moscow Region 142432, Russian Federation.